Journal Name

ARTICLE TYPE

Cite this: DOI: 10.1039/xxxxxxxxxx

High-Resolution Nuclear Magnetic Resonance Spectroscopy in Microfluidic Droplets

William Hale,[a] Gabriel Rossetto,[a] Rachael Greenhalgh,[a†] Graeme Finch,[a,‡] and Marcel Utz[a*]

Received Date
Accepted Date

DOI: 10.1039/xxxxxxxxxx

www.rsc.org/journalname

A generic approach is presented that allows high-resolution NMR spectroscopy of water/oil droplet emulsions in microfluidic devices. Microfluidic NMR spectroscopy has recently made siginficant advances due to the design of micro-detector systems and their successful integration with microfluidic devices. Obtaining NMR spectra of droplet suspensions, however, is complicated by the inevitable differences in magnetic susceptibility between the chip material, the continuous phase, and the droplet phases. This leads to broadening of the NMR resonance lines and results in loss of spectral resolution. We have mitigated the susceptibility difference between the continuous (oil) phase and the chip material by incorporating appropriately designed air-filled structures into the chip. The susceptibilities of the continuous and droplet (aqueous) phases have been matched by doping the droplet phase with a Eu^{3+} complex. Our results demonstrate that this leads to a proton line width in the droplet phase of about 3 Hz, enabling high-resolution NMR techniques.

Introduction

NMR spectroscopy is one of the most important analytical tools available to chemistry, biochemistry, and the life sciences. Due to its linearity and generality, it is particularly suited to quantify metabolic compounds in biological systems.[1,2] At the same time, microfluidic technology is rapidly evolving, enabling numerous novel applications in chemistry and the life sciences. Droplet microfluidics is based on the separation of samples into small droplets suspended in an inert transport fluid (often a fluorinated oil).[3–6] In this way, samples can be manipulated freely in the lab-on-a-chip (LoC) system, and problems due to viscous dispersion and cross-contamination are avoided. For example, several groups have reported encapsulation of cells into individual droplets.[7,8] Droplets can efficiently be sorted according to numerous chemical and biochemical criteria by the help of suitable fluorescent markers. As a result, droplet microfluidic systems are increasingly finding applications in chemistry[9] and the life sciences.[8,10] In this paper, we explore the possibility to obtain high-resolution NMR spectra from small volumes of droplet emulsions on a chip. Integration of high-resolution NMR spectroscopy with microfluidic systems is challenging for a number of reasons. On the one hand, small sample volumes place stringent demands on detector sensitivity.[11,12] This has recently been addressed with the design of highly efficient planar NMR microcoils[13] and transmission line resonators.[14] Another challenge is the preservation of high spectral resolution, which depends on a highly homo-

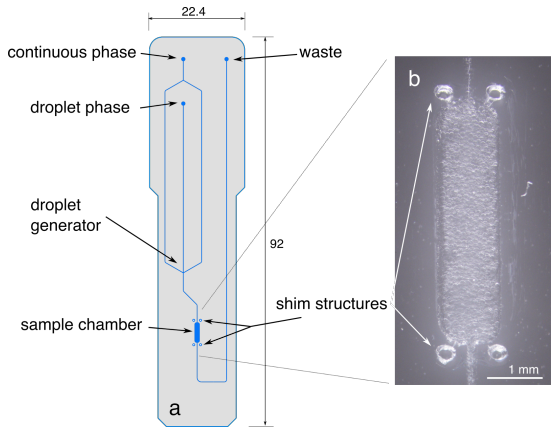

Fig. 1 Droplet chip design (left) and detail micrograph of the sample chamber area filled with droplets (right). Some droplets are also visible in the entrance and exit channels.

[a] *School of Chemistry, University of Southampton, Southampton SO17 1BJ, United Kingdom. E-mail: marcel.utz@southampton.ac.uk*

† Present address: Department of Chemistry, Loughborough University, United Kingdom

‡ Present address: National Physical Laboratory, Hampton Road, Teddington, Middlesex TW11 0LW, United Kingdom

geneous magnetic field over the sample volume. Differences in magnetic susceptibility between the materials used for the microfluidic chip and the sample fluid, as well as the materials and geometry of the probe assembly, lead to a demagnetising field that varies continously over the sample volume. Typical diamagnetic volume susceptibilties range from about -11 ppm to about -5 ppm (in SI units);[15,16] differences of the order of several ppm are therefore commonplace. Unmanaged, they lead to broadening of NMR spectral lines over a ppm or more, which corresponds to a severe loss of resolution in ^{1}H liquid state NMR.

In emulsions, susceptibility differences between the oil and aqueous phases lead to similar line broadening.[15] NMR spectroscopy is extensively used to characterise emulsion droplet size distributions using pulsed field gradient methods.[17–23] These methods do not require spectral resolution of individual compounds other than the two solvents, and are therefore unaffected by the susceptibility broadening. By contrast, high-resolution NMR spectroscopy, with sufficient resolution to distinghuish multiple compounds present in either of the two phases, requires careful mitigation of the susceptibility differences.

We have recently shown that it is possible to compensate for susceptibility differences between microfluidic chips and the sample fluid by incorporating appropriately shaped shim structures into the chip design.[24] These structures are filled with air, and are shaped in such a way as to cause demagnetising fields that are equal and opposite to those caused by the sample/chip interface. It has also been shown that susceptibility differences can be compensated for in a liquid sample by doping of a chelated lathanide.[25] For example, Lennon *et al.* demonstrated that the susceptibility mismatch between the inside and outside of deoxygenated red blood cells could be compensated for by doping 3mM of dysprosium tripolyphosphate ($Dy(PPP)_2^{7-}$) into the extracellular fluid.[26]

Managing susceptibility differences for an emulsion of droplets on a microfluidic chip adds additional complexity, since three different materials are now involved: the chip, the continuous phase, and the droplet phase, all with different susceptibilities. In the following, we show that this can be mitigated in a two-step approach, which is based on the observation that most organic solvents in use as continuous phases for droplet microfluidics are less diamagnetic than water. First, the susceptibility difference between the chip and the continuous phase are compensated by shimming structures that are added to the chip design. Then, the susceptibility of the aqueous droplet phase is matched to that of the continuous phase by adding a paramagnetic solute.

It should be noted that in principle, the same effect could be achieved if a diamagnetic dopant could be added to the continuous phase. However, while paramagnetic dopants are easily available in the form of transition metal ions, no effective diamagnetic dopants exist to our knowledge.

Eu^{3+} complexes are paramagnetic, and are frequently used as shift agents in NMR spectroscopy. Unlike other lanthanide ions such as Gd^{3+} or Ho^{3+}, which are powerful nuclear relaxation agents, Eu^{3+} has only a minimal effect on nuclear magnetic relaxation due to its extremely short electron spin-lattice relaxation time.[27] Addition of millimolar quantities of Eu^{3+} to aqueous solutions therefore does not cause significant relaxation line broadening, but changes the bulk magnetic susceptibility of the solution proportionally to the Eu^{3+} concentration. It is therefore possible to adjust the susceptibility difference in a droplet emulsion by adding a Eu^{3+} complex that selectively dissolves in (or at least strongly partitions to) the aqueous phase.

In the present work, we use the diethyl-triamine pentaacetate (DTPA) complex of Eu^{3+}, $Eu[DTPA]^{2-}$. As an ion species, it is readily soluble in aqueous media, while exhibiting only negilgible solubility in apolar organic solvents. Microfluidic chips are fabricated from poly methyl methacrylate (PMMA). By a fortunate coincidence, the suceptibilities of PMMA and water are very close to each other (Table 1). NMR lines in microfluidic devices made from PMMA are therefore narrow if aqueous samples are used, provided that the boundaries of the chip and the environment are either aligned with the external magnetic field, or are kept sufficiently remote from the detection area. By contrast, most organic

Table 1 Bulk magnetic susceptibilities

Compound	$\chi_V/10^{-6}$ (SI)	Ref
water	-9.05	28
cyclohexane	-7.640	28
PMMA	-9.01	29
Air	$+0.36$	30

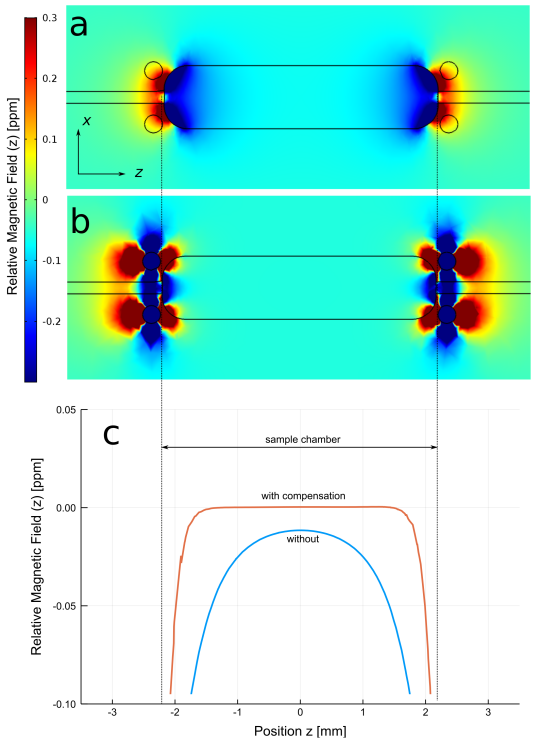

Fig. 2 A: Finite element simulation of relative magnetic field distribution in an uncompensated chip (circular structures filled with PMMA) filled with cyclohexane and B: a compensated chip filled with cyclohexane; C: a linear plot of relative magnetic field along the z-axis through the middle of the sample chamber.

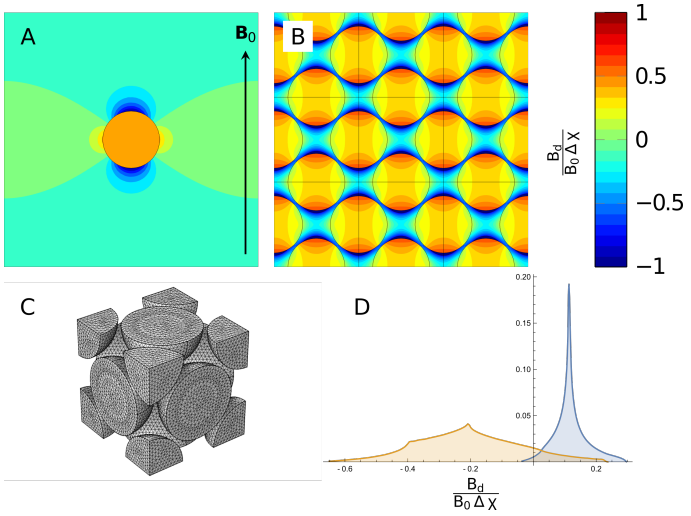

Fig. 3 A: Finite element simulation of magnetic field distribution in droplets. z-component of the reduced magnetic field H_{red} in an isolated spherical droplet and B: in a face-centred cubic arrangement of droplets; C: FEM mesh used to calculate the result shown in B; D: histograms of the z-component of the reduced magnetic field in the continuous (orange) and in the droplet (blue) phase in the FCC arrangement.

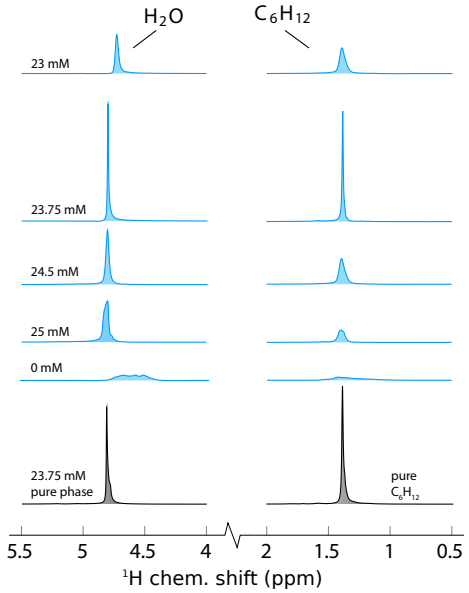

Fig. 4 1H NMR line shapes of water (left) and cyclohexane (right) of a water in cyclohexane emulsion as a function of $Eu[DTPA]^{2-}$ concentration in the aqueous phase normalised to the sharpest peak. The spectra given in black are the pure phase spectra produced by the same chip.

solvents are considerably less diamagnetic than water, as exemplified by the case of cyclohexane, which has been used in the present study.

In the remainder of this paper, we first use finite element calculations to estimate the NMR line widths expected in a droplet emulsion depending on the susceptibility mismatch. The results are then compared to experimental line widths obtained with varying concentrations of $Eu[DTPA]^{2-}$ in the aqueous phase. Finally, we show that narrow NMR lines can be obtained by combining structural shimming[24] with susceptibility matching, and demonstrate that this approach can be used to obtain a high resolution of glucose contained within the compensated droplets. The chip used in this work is shown in Fig. 1. It consists of a sample chamber in the centre of the chip, which is designed to line up with the sensitive area of a transmission-line micro-NMR detector,[14] and a convergent flow droplet generator. The aqueous phase and the continuous phase are fed into the two ports at the top. Droplets are formed and transported downstream into the sample chamber. The chamber is surrounded by four shim structures, which are circular shaped cutouts filled with air. They have been designed to compensate for the difference in susceptibility between the chip material (PMMA) and the oil phase (cyclohexane) as shown in Fig. 2. The operation of the chip is shown on the right side of Fig. 1; droplets of about 100 μm diameter are formed and fill the sample chamber.

Materials and Methods

Microfluidic chips of the design shown in Fig. 1 were fabricated from PMMA sheet material by laser cutting, and subsequent bonding of layers with a plasticiser under heat and pressure.[31] The chips consist of a top and bottom layer of 200 μm thickness each, and a middle layer of 500 μm. Fluid channels upstream from

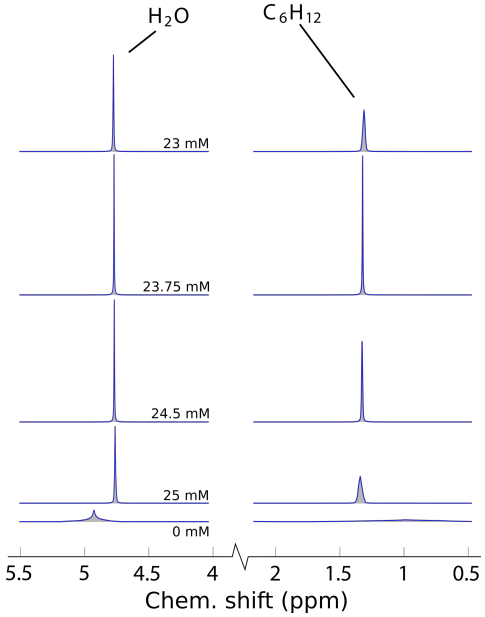

Fig. 5 Predicted ^{1}H NMR line shapes of water (left) and cyclohexane (right) of a water in cyclohexane emulsion as a function of $Eu[DTPA]^{2-}$ concentration in the aqueous phase.

the flow-focussing droplet generator were scored into the middle layer at low laser power to a depth of about 100 μm. Downstream from the droplet generator, the channels and the sample chamber were cut through the 500 μm middle layer by increased laser power, as were the shimming structures. The chips were connected to a pair of Cole-Palmer 200-CE syringe pumps for droplet generation. A flow rate of 20 μl/min was typically used for the continuous phase and 4 μl/min for the aqueous droplet phase. The continuous phase consisted of cyclohexane (Sigma-Aldrich) with 0.5% w/v of span-65 (sorbitan tristearate, Sigma-Aldrich) as a surfactant to ensure droplet stability. The cyclohexane/span solution was kept in a water bath at 30° degrees for at least 2h to ensure complete dissolution of the span. Prior to use, all solutions were left to equilibrate at a controlled room temperature of 25°C for at least 4h. Steady state conditions were ensured by letting the droplet generation run until the volume inside the chip had been exchanged at least five times. The chip was then disconnected from the syringe pumps, and the connection points sealed prior to insertion of the chip into the NMR probe.

NMR measurements were carried out on a Bruker AVANCE III spectrometer equipped with an Oxford wide bore magnet operating at 7.05 Tesla, corresponding to a ^{1}H Larmor frequency of 300 MHz. A home-built NMR probe based on a transmission-line detector was used.[14] It accommodates microfluidic chips of the shape shown in Fig. 1. In the present work, the probe was doubly tuned to allow irradiation both at 300 MHz for ^{1}H and at 75 MHz for ^{13}C. Details of the electronic and mechanical design of the probe are given in Ref.[32].

NMR spectra were obtained at an RF nutation frequency of 66 kHz for ^{1}H, corresponding to 90 degree pulse length of 3.8 μs. Shimming of the sample was first performed on a sample of pure cyclohexane in an identical chip, these resulting values were used throughout all subsequent experiments with minor adjustments being made to linear shims (X,Y,Z) before each experiment to minimise line width. NMR spectra were acquired using Bruker spectrometer software (TopSpin 2.0), and were processed using home-built scripts written in *Julia*.[33] 20 mM of 4,4-Dimethyl-4-silapentane-1-sulfonic acid (DSS, Sigma Aldrich) was added to the aqueous phase as a chemical shift standard.

MRI gradient echo images of the sample chamber were obtained using ParaVision software and the fast low-angle shot (FLASH) pulse program. Flip angles of 30° were employed as well as a repetition time of 600 ms; 8 scanes were averaged for each image. Two images were acquired for each field map at echo times of 6 and 10ms, respectively. The data was processed using home built software in *Mathematica*.

Eu[DTPA]$^{2-}$ solutions were prepared from a 82.2 ± 0.25 mM stock solution, which was prepared by adding 1 g of $EuCl_3$ (Sigma Aldrich) to a 50 mL volumetric flask. Separately, 3.93 g of diethylenetriaminepentaacetic acid (DTPA, Sigma Aldrich) and 1.99 g of NaOH (Fischer) were dissolved in 100 mL deionised (DI) water (Sigma Aldrich) . An equimolar amount of the DTPA solution was added to the $EuCl_3$ solution. The pH of this solution was then adjusted by addition of 2M NaOH solution dropwise until a neutral pH was attained. This was then topped up to 50 mL using DI water.

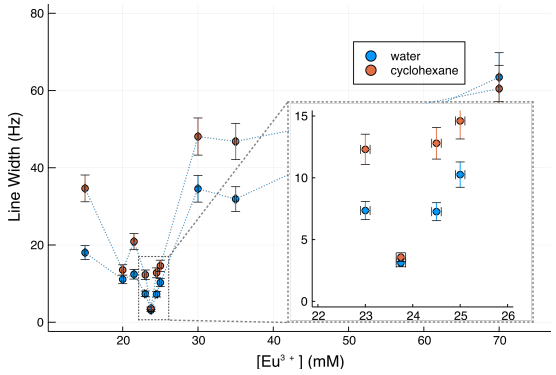

Fig. 6 Observed line widths of water (blue circles) and cyclohexane (orange circles) in microfluidic droplet emulsions as a function of the Eu[DTPA]$^{2-}$ concentration in the aqueous phase. Inset is the plot around the minimum concentration. The widths of both lines are minimal at the matched concentration of 23.75 mM.

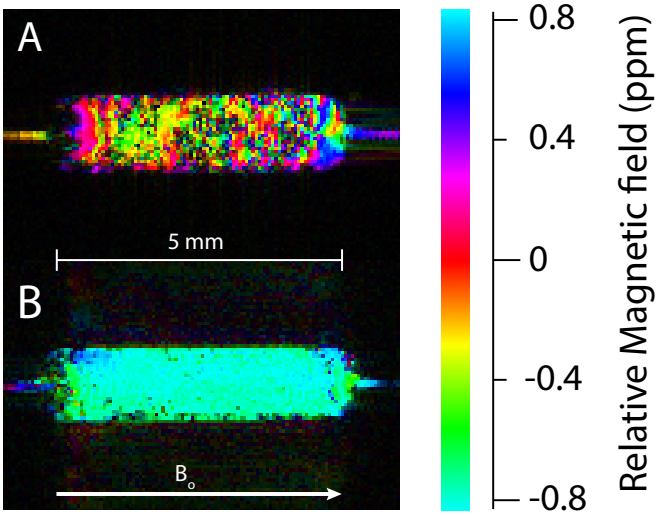

Fig. 7 B_0 field maps obtained by magnetic resonance imaging of emulsions with (A) $\Delta\chi = -1.41 \times 10^{-6}$ and (B) $\Delta\chi \approx 0$.

Finite element calculations of field distributions in emulsions were carried out using COMSOL 5.2a with the "magnetic fields, no currents" (mfnc) physics module. Optimisation of the shim structures was done with COMSOL 5.3. Starting from a SolidWorks model of the chip design, which was also used as a basis for production of the devices using a laser cutter, a finite element model was assembled and meshed. The shim structures consist of four symmetrically arranged circular holes through the middle layer of the three-layered devices. The positions and the diameters of these holes were optimised using a Nelder-Mead simplex algorithm. At each iteration, the magnetic field distribution inside the sample chamber was calculated using the mfnc physics module. The square norm of the second derivative of the z-component of the magnetic field was integrated over the volume of the sample chamber, and was used as optimisation target.

Results and Discussion

While it is possible to predict the magnetic field distribution in a system of multiple phases with differing susceptibilities by solving the magnetostatic equation, this requires precise geometric information on the arragement of the two phases. In the case of an emulsion, the arrangement of the droplets is not regular. However, at high droplet densities, it can be expected to approximate a dense packing of spheres. In order to obtain a semi-quantitative prediction, we have computed the demagnetising field in face-centred cubic (FCC) and simple cubic (SC) lattices of diamagnetic spheres; the results are shown in Fig. 3. A single unit cell containing one (SC) or two (FCC) independent spheres was meshed under periodic boundary conditions in all directions (Fig. 3C). As is well known, the demagnetising field inside an isolated diamagnetic sphere is homogeneous, while the field outside of the sphere is that of a magnetic point dipole located at the sphere's centre. This situation is approximated in a lattice if the lattice constant is much larger than the sphere diameter. The computed demagnetising field of a small sphere in an SC lattice is shown in Fig. 3A. The contour levels display the z-component of the local demagnetising field normalised by the background B_0 field and the susceptibility difference $\Delta\chi = \chi_{\text{sphere}} - \chi_{\text{continuous}}$. The field is homogeneous inside the sphere, and a spatially varying demagnetising field only exists in the continuous phase. By contrast, in a densely packed face-centered cubic lattice the field is no longer homogeneous inside the spheres (Fig. 3B). The FCC lattice approximates the geometry of a dense microemulsion of homogenous water-in-oil droplets. Fig. 3D shows the histograms of the z-components of the demagnetisig field in the continuous and droplet phases of the FCC lattice, respectively.

The NMR spectra expected from an ideal emulsion of the same geometry can be predicted from these histograms (neglecting no broadening contributions from the sample container). The magnetic field relevant for nuclear Larmor precession, often referred to as the "external" field[34] $\mathbf{B}_{\text{ext}}$ is given by[24]

$$\mathbf{B}_{\text{ext}}(\mathbf{r}) = B_0(1 + \frac{\chi_s}{3})\mathbf{e}_z - \mu_0 \nabla U_d(\mathbf{r}), \quad (1)$$

where B_0 is the magnitude of the external field, χ_s is the local magnetic susceptibility, and $U_d(\mathbf{r})$ is the scalar magnetic potential of the demagnetising field. The volume susceptibility of a solution containing a paramagnetic species at low concentration c_p is

$$\chi_s \approx \chi_0 + c_p\,\zeta_P, \quad (2)$$

where χ_0 is the volume susceptibility of the pure solvent, and ζ_P is the molar susceptibility of the paramagnetic species. ζ_P depends slightly on the molecular environment. For example, values of $5.86 \cdot 10^{-5}$ l/Mol, $5.68 \cdot 10^{-5}$ l/Mol, and $6.14 \cdot 10^{-5}$ l/Mol have been measured at 300K for Eu_2O_3, EuF_3, and $EuBO_3$, respectively.[35] To our knowledge, the precise molar susceptibility of $Eu[DTPA]^{2-}$ in aqueous solution has not been measured to date, but it is likely to be similar to the above values.

Fig. 4 shows ^{1}H NMR spectra obtained from emulsions in the chip shown in Fig. 1 with varying $Eu[DTPA]^{2-}$ concentrations in the aqueous phase as indicated in the figure. While the spectra are extremely broad without dopant, concentrations in the vicinity of 23 mM lead to much sharper lines for both water and cyclohexane, and the pure phase line widths are recovered at the optimum concentration of $c_p = 23.75$ mM. Using the susceptibilities given in Table 1, this leads to molar susceptibility for $Eu[DTPA]^{2-}$ of $5.94 \cdot 10^{-5}$ l/Mol, well within the range of molar susceptibilities reported in literature for other Eu^{3+} compounds. Using this value, the histograms shown in Fig. 3D can be converted into predicted emulsion NMR spectra as a function of $Eu[DTPA]^{2-}$ concentration in the aqueous phase, as shown in Fig. 5. The predicted behaviour is qualitatively similar to the experimental observation; very broad lines are expected at zero dopant concentration, while sharp lines are recovered near the optimum concentration. Also, the droplet phase peak is predicted to be narrower than the one from the continuous phase; this is already evident in the histograms in Fig. 3. However, the predicted spectra are consistently sharper than the experimentally observed ones. It is not entirely clear what causes the discrepancy between the experimental observation and the simulations. However, it should be noted that the experimental geometry of the emulsion differs significantly from the simulation; the droplets are neither uniform in size, nor are they arranged in a crystalline (FCC) lattice.

The observed widths of the NMR signals from cyclohexane and water are summarised in Fig. 6. Here, we define the line width as the ratio of the peak integral to the peak height, multiplied by $2/\pi$. In the case of Lorentzian line shapes, this definition is equivalent to the full width at half height (FWHM). However, the expected line shapes from the droplet emulsion are very different from a Lorentzian (Fig. 3D), such that using the FWHM would be misleading.

Both line widths exhibit a narrow minimum at 23.75 mM $Eu[DTPA]^{2-}$ in the aqueous phase. The water and cyclohexane minimum peak widths are 3.1 Hz and 3.5 Hz, respectively. For comparison, the best resolution that has been reached with the same NMR probe is 1.76 Hz for a homogeneous solution of 150 mM sodium acetate in H_2O.[14]

Fig. 7 shows magnetic field (B_0) maps are shown of sample chambers filled with droplet emulsions. In these experiments, two separately images with different echo times are acquired. The phase difference in each pixel is proportional to the echo time difference and to the local magnetic field. The colour denotes the phase acquired by each pixel and can be used to inform on the homogeneity of the magnetic field in the sample.

In Fig. 7A, the droplets do not contain any paramagnetic dopant. As a result, the susceptibilities of the phases are unmatched, and strong local magnetic field differences are visible in the images. By contrast, the droplets in Fig. 7B are doped with 23.75 mM $Eu[DTPA]^{2-}$. As is clearly visible in the image, the local differences in the magnetic fields are strongly attenuated in this case.

While the above results have demonstrated that optimal line widths can be minimised in ^{1}H NMR spectra of microfluidic emulsions by paramagnetic doping, the question remains if this is sufficient to resolve homonuclear J-couplings of a few Hz. This is required in order to do meaningful NMR spectroscopy, particularly in the context of complex metabolic mixtures. The top trace

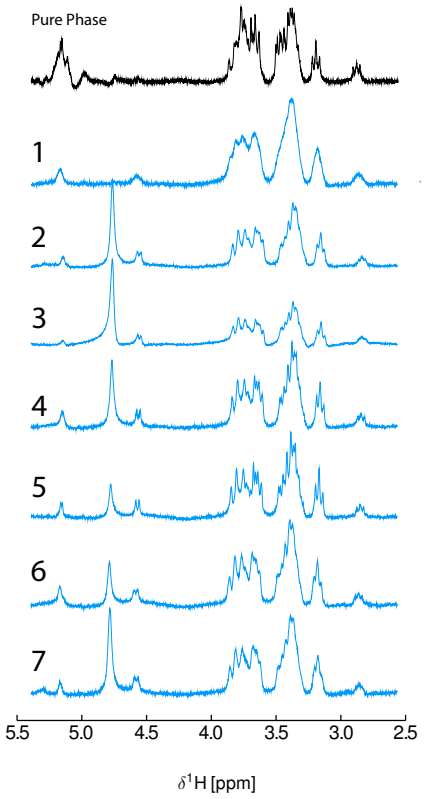

Fig. 8 Spectra of 200 mM Glucose in H_2O obtained from microfluidic droplet emulsions in cyclohexane. 1: Aqueous phase contains $c_0 = 23.75 \pm 0.25$ mM Eu[DTPA]$^{2-}$. Spectra 2-7 have been obtained by gradual dilution of the aqueous phase with small amounts of DI water. 2: $\ln c/c0 = -0.5\%$; 3: $\ln c/c0 = -0.75\%$; 4 : $\ln c/c0 = -0.875\%$; 5 : $\ln c/c0 = -1.0\%$; 6 : $\ln c/c0 = -1.125\%$; 7 : $\ln c/c0 = -1.25\%$. A spectrum of pure phase 200mM glucose with optimised Eu doping in the same chip is included for comparison (black). The nonuniform peak at 4.8 ppm is due to carrier frequency drift during water suppression

in Fig. 8 shows a spectrum of 200 mM glucose and 23.75 mM Eu[DTPA]$^{2-}$ in water. The water signal has been suppressed by pre-saturation. In this case, the resolution is about 3 Hz; such that e.g., the triplet at 3.2 ppm (which corresponds to the proton in the 2-position on the β-glucose anomer) is clearly resolved.

Spectrum 1 in Fig. 8 has been obtained from droplet emulsions, starting form an aqueous stock solution prepared to a nominal concentration of 23.75 mM in Eu[DTPA]$^{2-}$ and 200 mM in glucose. To our initial disappointment, the resolution in this spectrum is quite poor, in spite of the attempt to dope at the previously determined optimum concentration. However, we estimate the pipetting and weighing errors to add up to an uncertainty in the concentration of the stock solution of $\pm 1\%$. Assuming the stock solution was too concentrated, rather than too dilute, it was then gradually diluted with small amounts of DI water corresponding to a change in concentration much less than the experimental error in each step. As can be seen in spectra 2-7, the resolution gradually increases, and matches that of the pure phase spectrum at spectrum 5, before it deteriorates again. In practice, high resolution spectra therefore require careful calibration of the dopant concentration. It may not be practical to achieve this in one step by preparing the stock solution, particularly if small volumes (around 10 ml or so) are used as in our experiments. Rather, a gradual dilution as in Fig. 8 may be required to calibrate the Eu[DTPA]$^{2-}$ concentration for an accurate match of the aqueous and carrier fluid susceptibilities. However, if such a match is established, the resulting resolution is as good as that of the pure aqueous solution.

In summary, we have shown that the susceptibility differences between the chip, the aqueous phase, and the oil phase in a microfluidic droplet system can be successfully mitigated by a combination of structural shimming and doping of the less diamagnetic of the liquid phases with a europium compound. The ultimate resolution achieved is only slightly inferior to what has been demonstrated in homogeneous solutions on a microfluidic chip and is suitable for high resolution NMR spectroscopy.

This work has been supported by the 7th EU Framework programme through a Marie Curie Career Integration Fellowship to MU, and by the Horizon 2020 FETOPEN project TISuMR. The authors are grateful to Visvaldis Buns and Ali Yilmaz for help with manufacturing of the microfluidic chip.

References

1 N. Aranibar, M. Borys, N. A. Mackin, V. Ly, N. Abu-Absi, S. Abu-Absi, M. Niemitz, B. Schilling, Z. J. Li, B. Brock, R. J. I. Russell, A. Tymiak and M. D. Reily, *Journal of Biomolecular NMR*, 2011, **49**, 195–206.
2 D. S. Wishart, *TrAC Trends in Analytical Chemistry*, 2008, **27**, 228–237.
3 T. Thorsen, R. W. Roberts, F. H. Arnold and S. R. Quake, *Phys Rev Lett*, 2001, **86**, 4163–4166.
4 S. L. Anna, N. Bontoux and H. A. Stone, *Applied Physics Letters*, 2003, **82**, 364–366.
5 A. Günther and K. Jensen, *Lab Chip*, 2006, **6**, 1487–1503.
6 P. Garstecki, M. J. Fuerstman, H. A. Stone and G. Whitesides, *Lab Chip*, 2006, **6**, 693–693.
7 T. P. Lagus and J. F. Edd, *J. Phys. D Appl. Phys.*, 2013, **46**, 114005.
8 L. Mazutis, J. Gilbert, W. L. Ung, D. A. Weitz, A. D. Griffiths and J. A. Heyman, *Nat Protoc*, 2013, **8**, 870–891.
9 A. B. Theberge, E. Mayot, A. El Harrak, F. Kleinschmidt, W. T. S. Huck and A. D. Griffiths, *Lab Chip*, 2012, **12**, 1320–1326.
10 Y. Zhu and Q. Fang, *Analytica Chimica Acta*, 2013, **787**, 24–35.
11 V. Badilita, R. C. Meier, N. Spengler, U. Wallrabe, M. Utz and J. G. Korvink, *Soft Matter*, 2012, **8**, 10583–10597.
12 S. S. Zalesskiy, E. Danieli, B. Blümich and V. P. Ananikov, *Chem. Rev*, 2014, **114**, 5641–5694.
13 N. Spengler, J. Höfflin, A. Moazenzadeh, D. Mager, N. MacKinnon, V. Badilita, U. Wallrabe and J. G. Korvink, *Plos One*, 2016, **11**, e0146384.
14 G. Finch, A. Yilmaz and M. Utz, *Journal of Magnetic Resonance*, 2016, **262**, 73–80.
15 P. W. Kuchel, B. E. Chapman, W. A. Bubb, P. E. Hansen, C. J. Durrant and M. P. Hertzberg, *Concepts in Magnetic Resonance Part A*, 2003, **18A**, 56–71.
16 C. J. Durrant, M. P. Hertzberg and P. W. Kuchel, *Concepts Magn. Reson.*, 2003, **18A**, 72–95.
17 J. C. VANDENENDEN, D. WADDINGTON, H. VANAALST, C. G. VANKRALINGEN and K. J. PACKER, *Journal of Colloid and Interface Science*, 1990, **140**, 105–113.
18 I. FOUREL, J. P. GUILLEMENT and D. LEBOTLAN, *Journal of Colloid and Interface Science*, 1994, **164**, 48–53.
19 K. G. Hollingsworth, A. J. Sederman, C. Buckley, L. F. Gladden and M. L. Johns, *Journal of Colloid and Interface Science*, 2004, **274**, 244–250.
20 J. P. Hindmarsh, J. H. Su, J. Flanagan and H. Singh, *Langmuir*, 2005, **21**, 9076–9084.
21 M. L. Johns, *Current Opinion in Colloid & Interface Science*, 2009, **14**, 178–183.
22 R. Bernewitz, G. Guthausen and H. P. Schuchmann, *Magnetic Resonance in Chemistry*, 2011, **49**, S93–S104.
23 I. A. Lingwood, T. C. Chandrasekera, J. Kolz, E. O. Fridjonsson and M. L. Johns, *Journal of Magnetic Resonance*, 2012, **214**, 281–288.
24 H. Ryan, A. Smith and M. Utz, *Lab Chip*, 2014, **14**, 1678–1685.
25 M. E. Fabry and R. C. San George, *Biochemistry*, 1983, **22**, 4119–4125.
26 A. J. Lennon, N. R. Scott, B. E. Chapman and P. W. Kuchel, *Biophysical journal*, 1994, **67**, 2096–2109.

27 J. A. Peters, J. Huskens and D. J. Raber, *Progress in Nuclear Magnetic Resonance Spectroscopy*, 1996, **28**, 283–350.
28 *CRC Handbook of Chemistry and Physics*, ed. J. Rumble, 2017, pp. 1–4.
29 M. C. Wapler, J. Leupold, I. Dragonu, D. von Elverfeld, M. Zaitsev and U. Wallrabe, *Journal of Magnetic Resonance*, 2014, **242**, 233–242.
30 C. J. G. Bakker and R. de Roos, *Magn. Reson. Med.*, 2006, **56**, 1107–1113.
31 A. Yilmaz and M. Utz, *Lab Chip*, 2016, **16**, 2079–2085.
32 G. R. Finch, *PhD thesis*, University of Southampton, Southampton, 2017.
33 J. Bezanson, A. Edelman, S. Karpinski and V. B. Shah, *SIAM Rev.*, 2017, **59**, 65–98.
34 M. H. Levitt, *Concepts Magn. Reson.*, 1996, **8**, 77–103.
35 Y. Takikawa, S. Ebisu and S. Nagata, *Journal of Physics and Chemistry of Solids*, 2010, **71**, 1592–1598.